The Fundamental Research And New Concepts Compressor

LTF's new low-speed axial compressor test rig for atmospheric and sub-atmospheric operation

Daniel Jäger, Patrick Steudel, Volker Gümmer
daniel.jaeger@tum.de
Technical University of Munich
TUM School of Engineering and Design
Institute of Turbomachinery and Flight Propulsion
Garching bei München
Germany

ABSTRACT

This paper introduces the Fundamental Research And New Concepts Compressor *FRANCC* of the Institute of Turbomachinery and Flight Propulsion (LTF) at the Technical University of Munich (TUM). The compressor is a 3.5-stage low-speed axial research compressor designed to investigate new blading concepts, such as tandem and hybrid blades in a representative, multistage environment. The test rig features an inlet throttling system to lower the absolute pressure level to 250 mbar to investigate the influence of the Reynolds number on the blade's performance. The measurement system consists of fixed pressure and temperature instrumentation as well as a traversing system for aerodynamic probes downstream of each blade row. Besides the concept of the test rig, the testing and data processing methodology is presented in this paper. Following a commissioning phase, the first scientific test campaign using a configuration with conventional (single-blade) rotors and tandem stator vanes has now been completed, showing dependable results with high-quality resolution. Building on the tandem design and using the modularity of the test rig, further projects are already being planned and prepared.

Keywords: Low-Speed Compressor; Compressor Test Rig; Tandem Stator Vanes; Reynolds Number Variation

NOMENCLATURE

5HP	Five-hole probe
AC	Auxiliary compressor
AFB	Air-film bearing
CAD	Computer-aided design
CFD	Computational fluid dynamics
CTA	Constant temperature anemometry
DAQ	Data acquisition
FRANCC	Fundamental Research And New Concepts Compressor
GUI	Graphical user interface
HW	Hot-wire
IGV	Inlet guide vane
I/O	Input/output
ISO	International Organization for Standardization
LTF	Lehrstuhl für Turbomaschinen und Flugantriebe (Institute of Turbomachinery and Flight Propulsion)
OPC UA	Open Platform Communication - Unified Architecture
PC	Personal computer
PLC	Programmable logic control
RC	Research compressor
RANS	Reynolds-averaged Navier-Stokes equations
RMS	Root mean square

Symbols

c_p	Specific heat capacity at constant pressure in $\frac{\mathrm{J}}{\mathrm{kg \cdot K}}$
$\dot{m}$	Mass flow rate in kg/s
n	Rotational speed in 1/min
p_a	Absolute pressure in Pa
p_d	Differential pressure in Pa
p_t	Total pressure in Pa
T_t	Total temperature in K
R	Specific gas constant in $\frac{\mathrm{J}}{\mathrm{kg \cdot K}}$
γ	Isentropic exponent

1 INTRODUCTION

For decades, low-speed compressor testing has been an elaborated way for fundamental research of turbo compressors. The advantages of such a test rig compared to testing at relevant Mach numbers (high-speed testing) are numerous (cf., [1]):

- Reduced complexity of the test system, e.g., no secondary air system is needed.
- Low influence of the instrumentation and aerodynamic probes on the flow due to the large scale of the blades. This enables a detailed measurement resolution of the flow field and secondary flow phenomena.
- Easy accessibility.
- Low mechanical loads enable using cheap and easy-to-manufacture materials such as aluminum alloys.
- Low operational costs due to the relatively low power consumption.

On the other hand, the disadvantage is that compressibility effects (such as shock waves) cannot be covered in low-speed tests [1]. This makes a low-speed compressor test rig an optimal solution for fundamental turbomachinery research and early stages of development, where the focus is on the operational behavior and major flow characteristics rather than compressibility effects.

Many research organizations, both in industry and academia, operate low-speed test rigs, e.g., the Low-Speed Reseach Compressor (LSRC) operated by the *General Electric Company* [1], the low-speed test rig of NASA Lewis Research Center [2], the C106 and the Deverson test rig at Whittle Laboratory [3], the low-speed compressor (*Niedergeschwindigkeitsverdichter* - NGV) at Technische Universität Dresden [4], and the Low-Speed Large-Scale Axial Compressor (LSLSAC) test facility at Beihang University [5] to name a few examples around the globe. Frequently seen characteristics of these rigs are:

- Large scale with tip radii up to 762 mm ([1], [3]).
- Low rotational speeds around 1000 $\frac{1}{\text{min}}$ (except the C106 test rig).
- Single-stage setup or four geometrically identical compressor stages, both with an inlet guide vane (IGV).
- Constant channel height, which allows an easy exchange of the blades.
- Large variation of installable configurations, such as single-stage or multi-stage setups, cantilevered or shrouded stators, etc.
- Vertically aligned shaft ([1] and [4]).
- Extensive instrumentation, including wall pressure taps, pressure rakes, blade-surface instrumentation, and access for aerodynamic probes and optical measurement techniques.

During the last years, the Institute of Turbomachinery and Flight Propulsion (LTF) at the Technical University of Munich (TUM) has built the Fundamental Research And New Concepts Compressor *FRANCC* to test and validate new concepts of compressor blading. The main research focus is on investigating highly loaded concepts involving tandem and hybrid blades. The compressor is a 3.5-stage machine with geometrical relations and aerodynamic coefficients representative of the rear stages of high-pressure aero-engine compressors. This paper introduces the test rig, the design of the research compressor and, in detail, discusses the instrumentation and measurement system. A specialty of the test rig, which has not been found in the open literature yet, is the possibility to lower the inlet pressure of the research compressor with an inlet throttling system (operation under sub-atmospheric conditions) and, thus allowing a variation of the compressor's Reynolds number. In this paper, the term "blade" refers to both rotors and stators.

2 TEST RIG SETUP

The general schematic of the test rig is shown in Figure 1 and Figure 2: The test rig is split into two main parts, the actual research compressor (RC) and the auxiliary compressor (AC), which is necessary for operation under sub-atmospheric conditions. The parts are installed in dedicated rooms.

For atmospheric operation (Figure 1), the research compressor ingests air directly from the room through an inlet filter (not shown here, visible in Figure 5). Ambient air enters the room via an inlet silencer. The compressor itself is installed vertically to enable good accessibility and circumferential uniformity of the flow. An electric motor (M) drives the research compressor. At the compressor outlet, the air is collected in the volute (not shown). From there, it passes the mass flow sensor (flowmeter – FM) and then the outlet throttling system before being released to the environment through an exhaust silencer. The throttling system consists of a main throttle with a diameter of 600 mm and a bypass throttle of 200 mm for fine-tuning the throttling state. The main throttle is equipped with a fast-actuating pneumatic drive, which can open the throttle from 30 % to 100 % opening ratio in approx. 3 s. This drive, together with a second quick-opening

valve (anti-surge valve), which reacts within approx. 1 s, is responsible of recovering the compressor from stall. At the same location, the duct to the AC is connected, starting with the AC valve (shown in grey color), which is closed during atmospheric operation.

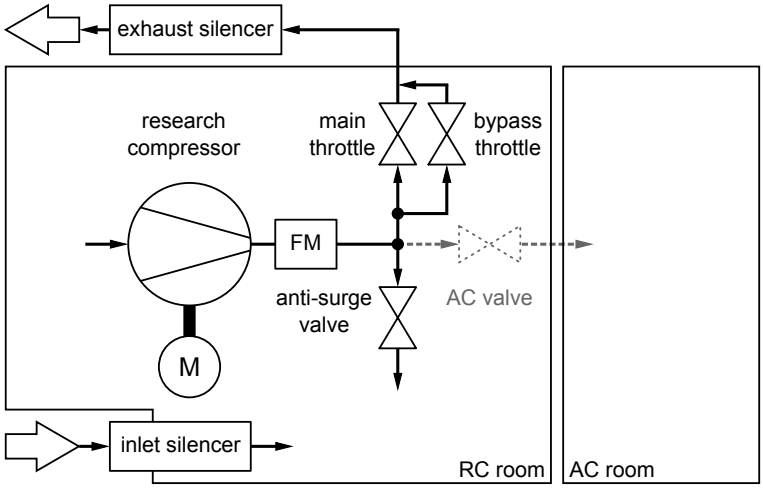

Figure 1 Schematic of the test rig for atmospheric operation

For sub-atmospheric operation (Figure 2), the air is not directly taken in from the room into the compressor but passes through an inlet throttling system, which allows lowering the absolute inlet pressure to 250 mbar, which is approx. 25 % of the ambient pressure. A settling chamber is then necessary to homogenize the flow before reaching the actual RC inlet. Exiting the compressor, the air does not pass the outlet throttling system (main and bypass throttle are closed) as it does for atmospheric operation. Instead, it is guided through the open AC valve to the neighboring room (AC room), where the auxiliary compressor is installed. The AC is a single-stage centrifugal compressor that raises the pressure to atmospheric conditions again before guiding the air to the exhaust silencer.

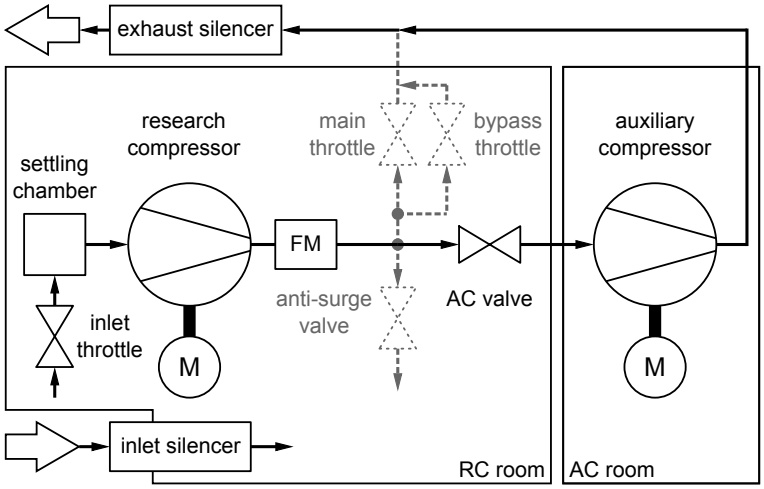

Figure 2 Schematic of the test rig for sub-atmospheric operation

Figure 3 shows a CAD model of the test facility in the configuration for sub-atmospheric operation. The RC room with the axial research compressor is located on the left side. A platform allows comfortable access to the RC around its entire circumference. The inlet throttling system is mounted to the walls of the RC room. A pipe system connects it with the settling chamber mounted on top of the RC. The intakes are mounted above the location where ambient air enters the room. The outlet throttling system is located in the rear top right corner of

the room (top center of the model). The AC room is located on the right side, containing the AC's drive train (electric motors and gearbox) and the AC itself. Several sub-systems, such as the RC's main drive and the oil supply systems for the AC and gearbox, are installed in the basement of the building (not shown).

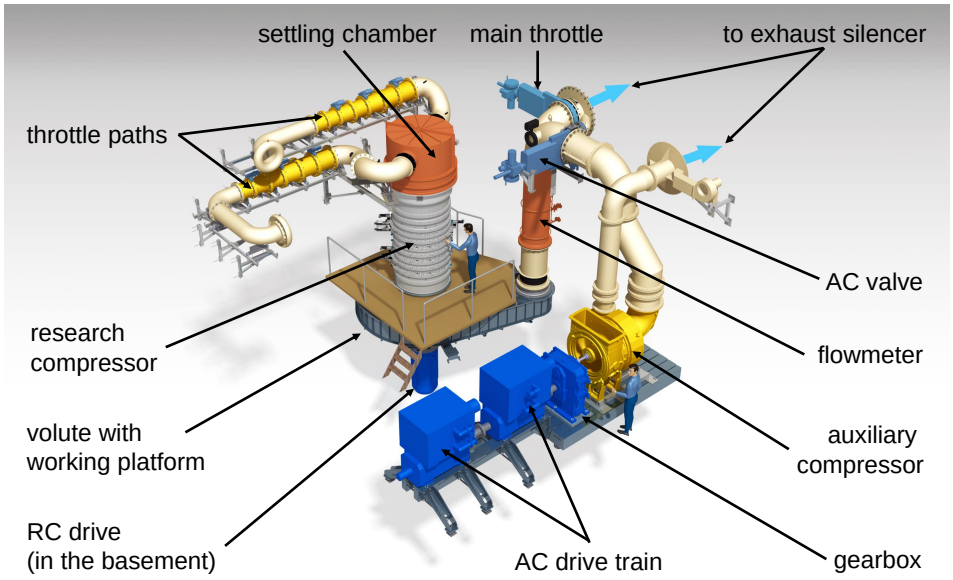

Figure 3 CAD model of the test rig for sub-atmospheric operation

3 RESEARCH COMPRESSOR

In this section, the design of the research compressor is discussed shortly. All information in this section refers to the currently installed gas path and blade geometries (build 1.0). A preliminary state of the aerodynamic design is reported in [6], although significant changes have been made after the publication of the paper. Dedicated numerical studies performed on the design are presented in [7] and [8].

The research compressor (RC) is a 3.5-stage low-speed axial compressor with geometrical relations representative for the rear stages of high-pressure aero-engine compressors. Figure 4 shows a meridional view of the gas path of build 1.0. The compressor consists of conventional (single-blade) rotors and shrouded stators in a tandem configuration. The three stages are geometrically identical. An inlet guide vane (IGV) installed upstream of the first rotor row provides a pre-swirl of the flow and, thus, an equal loading of each compressor stage. The gas path contracts throughout the rotors and expands throughout the tandem stators. The cavity underneath the stators is sealed with three sealing fins.

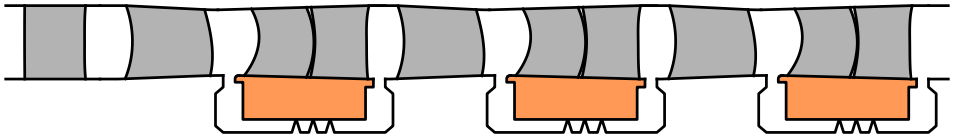

Figure 4 Meridional view of the gas path of the RC, build 1.0

Table 1 shows the main aerodynamic design parameters of the compressor (current blading, build 1.0). The number of blades was chosen to be equal for all blade rows. This choice has the advantage of significantly shorter calculation times for unsteady numerical simulations. It is possible in the low-speed machine due to the relatively small mechanical excitations.

Table 1
Aerodynamic design parameters of the RC, build 1.0

Quantity	Symbol	Value
Number of blades (IGV-R-S)	N	40-40-40
Tip radius	R_{tip}	550 mm
Hub-to-tip ratio	ν	0.8
Relative rotor tip gap	$\frac{h_{\mathrm{tip}}}{h_{\mathrm{channel}}}$	1.75 %
Relative stator sealing clearance	$\frac{h_{\mathrm{clear}}}{h_{\mathrm{channel}}}$	1.00 %
Corrected speed	n_{corr}	1485.24 1/min
Corrected mass flow rate	$\dot{m}_{\mathrm{corr}}$	17.95 kg/s
Total pressure ratio	Π_t	1.1188
Flow coefficient	φ	0.57
Work coefficient per stage	Ψ_{ht}	0.59
Mach number at stator 1 inlet	$Ma_{\mathrm{S1,in}}$	0.224
Reynolds number for stator 1	Re_{S1}	$\approx 750\,000$

The motivation to investigate this configuration is now shortly explained. For details, please refer to [6], [7], [8], and the publications mentioned hereafter. Generally, the development of aero-engines tends to design compact cores with high overall pressure ratios. This forces the development of compressor technology towards a weight reduction at the same pressure ratio or a higher overall pressure ratio at the same weight. Both cases require raising the pressure ratio per stage while maintaining a good efficiency level. Transferring this demand into non-dimensional values leads to a higher aerodynamic stage loading Ψ_{ht} at the same stage efficiency and working range as current designs. For conventional blading concepts, the achievable loading is limited. Revolutionary concepts such as tandem blades, if properly designed, were shown to have higher efficiencies at high loading levels than conventional designs [9].
The use of a tandem stator, consisting of two vanes per compressor row, also reduces the effective Reynolds number for each vane under identical aerodynamic conditions. However, for the given inflow turbulence intensity of 4.5 % in combination with the load split of the front and rear vane, no laminar separation is expected [10], [11]. This will also be investigated in future studies when a variation in Reynolds number is performed; see Section 4.

The research compressor is designed to investigate the operational behavior and the detailed steady-state and time-resolved flow fields. Although the pressure ratio given in Table 1 is very low, the most important non-dimensional aerodynamic parameters (φ, Ψ_{ht}, De-Haller number, Diffusion factor, Re [10]), except the Mach number, are representative for an aero-engine compressor and thus allow an easy transition of the obtained results into the industrial application. A similar configuration has already been tested in a single-stage setup by [12] at the low-speed compressor in Dresden. The multistage investigations performed at the *FRANCC* test rig aim to understand the influence of the rotor flow field on the tandem stator and the downstream influence of a tandem stator on the next rotor blade row.

A CAD model of the research compressor module is shown in Figure 5a and consists of the following components: In the inlet duct, the flow is accelerated. The inlet filter, which consists of a metal cage covered with G2 filter material, is mounted on top of the inlet duct. Downstream of the inlet duct, a grid is mounted in a section with straight end walls. This grid introduces a certain level of turbulence to the flow and thickens the boundary layer to provide inflow conditions representative of rear compressor stages. The compressor stages are placed downstream of the grid. The blades are manufactured from aluminum alloy in the institute's workshop. The gas path is formed by the platforms, which are integral parts of the blades. The rotor casing end wall is formed by exchangeable casing rings, so

there is no restriction to a constant flow channel, as this is the case for most of the other test rigs mentioned in Section 1. The compressor stages are followed by the volute, where the flow is turned 180 degrees. The volute is connected to the exhaust system by a flange. The figure also shows one mounted traversing unit for measurements with aerodynamic probes; see Section 6.2 for a detailed description. The compressor is driven by a variable-speed electric motor with a maximum shaft power of 315 kW. The mechanical power is transmitted from the electric motor to the compressor via a shaft.
For the bearing of the compressor rotor, two bearing options are available: Air-film bearings and ball bearings. Air-film bearings on both the upper and lower bearings offer very low friction losses, thus allowing precise performance measurements. The disadvantage is that the lower air-film bearing does not support the mechanical loads that occur during the stall of the compressor. Therefore, a more robust ball bearing at the lower bearing position is selected for the first test setup. The upper bearing is always equipped with an air-film bearing, but the lifetime is limited to a few stall cycles.
Figure 5b shows a picture of the RC room. The compressor is located in the center of the picture. On the left side, the cabinet containing the measurement system, and on the right side, the cabinet containing the control system and the computer network devices are visible.

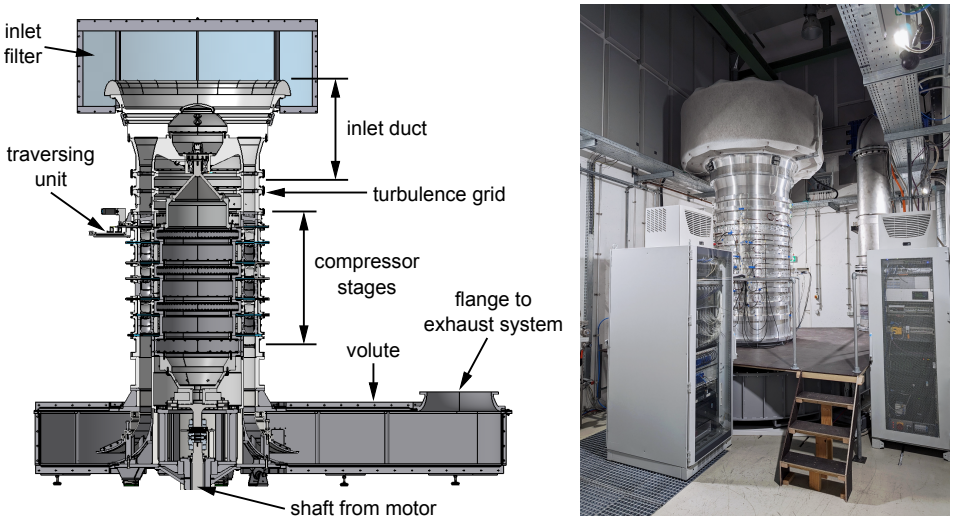

(a) CAD model of the RC module (b) Picture of the RC room

Figure 5 The research compressor

4 AUXILIARY COMPRESSOR AND SUB-ATMOSPHERIC OPERATION

To investigate the influence of the Reynolds number on new blading concepts such as tandem stator vanes, the compressor's absolute inlet pressure can be lowered to 250 mbar. This operational state is called sub-atmospheric operation in the context of this paper.

4.1 Inlet Throttling System

The throttling device aims to achieve a total pressure loss of the flow from ambient conditions (960 mbar) to the compressor inlet (p_t = 250 mbar). This should be continuously possible for an operating range of 2.8 kg/s to 5.5 kg/s. The pressure loss must take place in stages to avoid supersonic flows. A homogeneous inflow to the compressor with low turbulence is desired. To fulfill these requirements and

to meet the prevailing space conditions (especially the maximum ceiling height of the room), the throttling is divided into two streams of equal mass flow. Suitable flow conditions are then restored in a settling chamber, which is placed on top of the compressor inlet. See Figure 3 for a visual reference.

The throttling paths are designed using a 1-dimensional calculation. The pressure loss is achieved by a combination of different orifices. These are calculated according to the standards ISO 5167 part 1 [13] and 2 [14]. The validity range of this standard (pressure ratio of the orifice plate from 0.75 to 0.98) determines the minimum number of orifice plates required to be five. Six orifices are installed in order to use pairs of fixed and variable orifices. This combination is used to keep the throttle paths as short as possible. After a conventional orifice, the air jet is widened and homogenized again by the subsequent variable segmented orifices before the flow enters the next conventional one. The first orifice is designed as a perforated plate. The segmented orifices are designed with variable flow blockage in order to enable a continuous approach to the desired throttle position from the fully opened starting position.
The duct lengths and cross-section sizes of the individual sections of the throttle paths are first specified. These result from the space available at the test bench and the standard market sizes of the pipes to be used. To keep the Mach number low, a step-by-step increase in cross-section size has to take place. The starting point of the design process is the maximum mass flow. In an iterative calculation, the variable orifices are closed step-by-step until the target values of the minimum mass flow and the target pressure loss are reached. Values from the ISO standard [14] are used for the orifice plate calculation. Also, the segmented orifices and the perforated plate were estimated using the ISO standard by assuming a conventional orifice with the same area blockage. The stop criterion for the calculation is the maximum Mach number of 0.5 in the orifice.

A sectional view of a throttle path can be seen in Figure 6. The pairs of variable orifices and fixed orifices are clearly visible. The throttle path has a modular design and is mounted on rails. This allows the orifice plates to be replaced and adapted quickly.

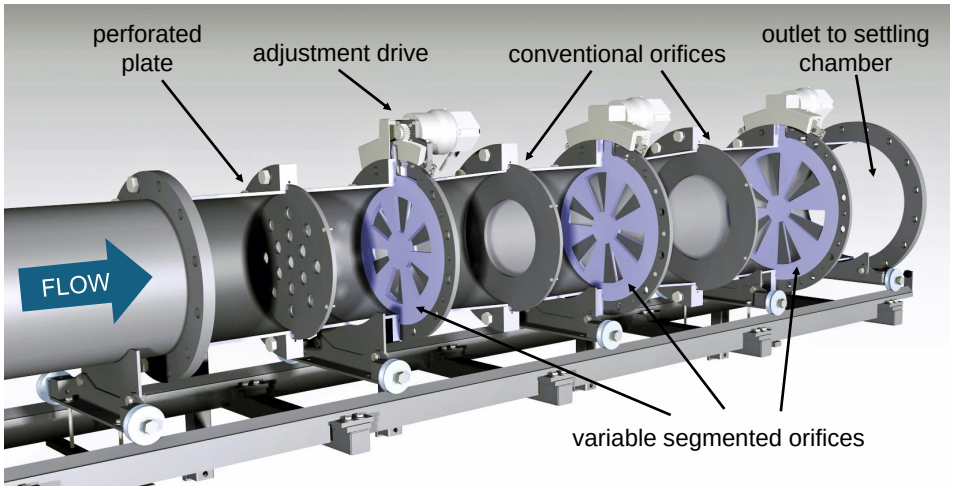

Figure 6 Sectional view of a throttle path

The air from the two throttle paths is then fed into a settling chamber placed on top of the compressor inlet; see Figure 3. The chamber was designed using CFD methods. The aim is to homogenize the flow before it enters the inlet and to reduce turbulence. This is achieved by the internal geometric design of the chamber, as well as a flow straightener and a turbulence screen.

4.2 Auxiliary Compressor

The total pressure ratio of the low-speed compressor is relatively small. Therefore, in sub-atmospheric operation, a second compressor, the auxiliary compressor, is necessary to raise the pressure of the exhaust air to ambient conditions again before being released into the environment. The auxiliary compressor is a single-stage centrifugal compressor from a modified marine turbocharger. The matching of research and auxiliary compressors is essential to provide a physically feasible system. Therefore, the matching process is explained here:
The challenge when matching the AC to the RC is the difference in the shape of the compressor maps of the two machines, which can be seen in Figure 7. Note that the original AC compressor map cannot be shown publically and is replaced here by a generic one of similar shape using the software *GasTurb 14* [15]. The centrifugal AC counts with a high maximum total pressure ratio but a relatively narrow compressor map at a specified pressure ratio. The reason is that the maximum mass flow is limited by choking flow. In contrast, the axial RC has a low total pressure ratio but a wide compressor map caused by the absence of a choke limit in the low-speed compressor. An additional constraint is given by the maximum output power of the AC's drive train, which is taken from a former test rig of the institute. The matching process itself is depicted in Figure 7 and consists of the following steps:

1. Assume a constant total inlet pressure for the RC, e.g. 250 mbar.
2. Compute the mass flow and total pressure ratio for a selection of points of the RC's compressor map. Compute the total pressure at the outlet of the RC.
3. Calculate the total pressure at the AC inlet considering losses in the piping system between RC and AC.
4. Calculate the required total pressure ratio of the AC when raising the pressure level to the ambient pressure. Losses in the outlet piping system are considered at this stage.
5. Draw the operating point (mass flow and total pressure ratio) into the AC's compressor map. Use the efficiency of the AC to compute the power demand.
6. Iteratively adjust the operating point of the AC while recalculating the total pressure losses in the outlet piping with the actual outlet temperature until convergence is reached.
7. Evaluate the operating point regarding the operating limits of the AC and the power constraint of the AC's drive train. The evaluation step can be seen in the compressor maps by the color code. Points colored in green can be covered by the AC. Points colored in red could be covered by the AC but exceed the power or torque constraint of the AC's drive train. Points colored in black cannot be covered by the AC.

The described procedure is repeated for different AC configurations and different total inlet pressures. The final selection of the AC is a modified *TCA 55* turbocharger from *MAN Energy Solutions SE*. The impeller is reduced in size to optimize the efficiency for the given operating points. Instead of the turbine section, a coupling to the electric drive train is attached to the compressor shaft. The drive train consists of two variable-speed electric motors of 400 kW shaft power each, in a serial dual-motor configuration. The rotational speed is increased by a gearbox with a ratio of approx. $10:1$.; see Figure 3.
As can be seen in Figure 7, not the entire compressor map of the RC can be covered by the AC. Due to the power constraints of the AC, the speed of the RC is limited to 80 % of the corrected design speed to limit the maximum mass flow. This limitation is deemed acceptable for the given low-speed flow conditions of the RC.

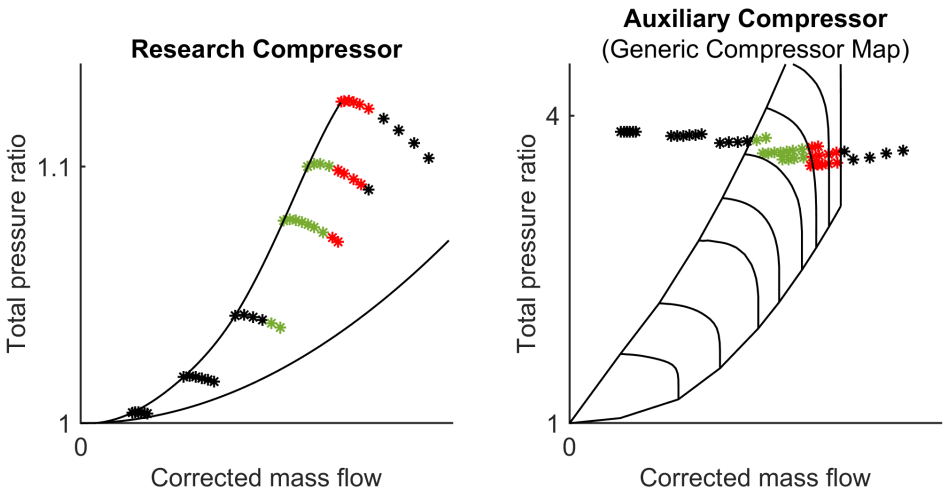

Figure 7 Matching process in the compressor maps of the RC and AC

4.3 Operational Strategy for Sub-Atmospheric Operation

As can be seen in Figure 7, very low mass flows cannot be covered by the AC with the full pressure ratio, i.e., an inlet throttling to 250 mbar. So, to put the rig into operation, the variable orifices of the inlet throttle are first fully opened, and then the opening ratio is sequentially reduced while increasing the rotational speeds of the RC and AC simultaneously. During the whole procedure, the operating points of the RC and AC have to be monitored closely so as not to exceed any limits. The sub-atmospheric operation focuses on investigating the performance and local changes in the flow field. The capabilities of the system cannot cover stall of the RC, so a sufficient stall margin has to be always maintained.

5 CONTROL SYSTEM

The test rig features a digital PC-based control system. The structure of the control system is depicted in Figure 8.

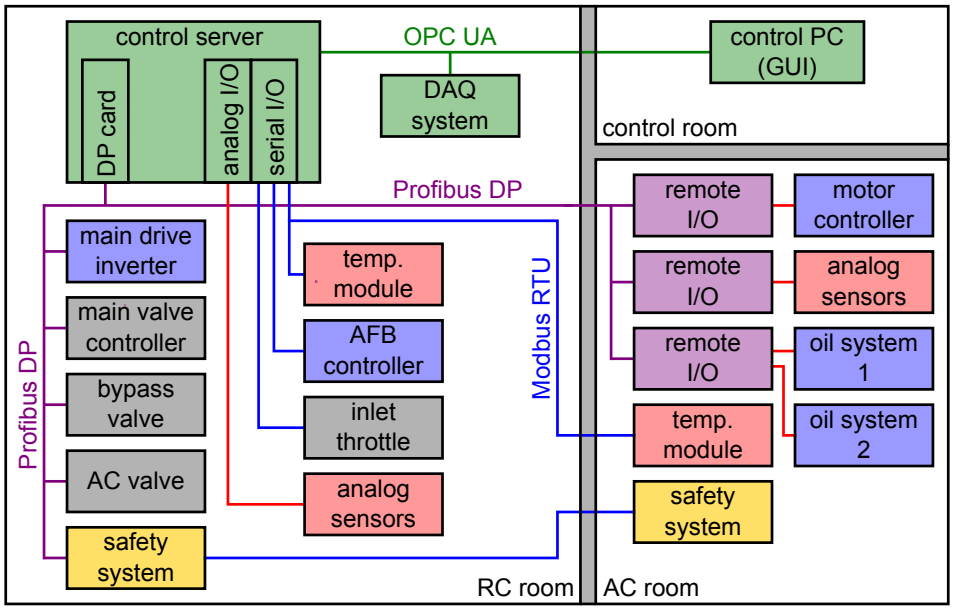

Figure 8 Structure of the control system

The control software, which is the core of the control system, runs on a Debian server and communicates with the sensors and actuators via different digital interfaces. The main drive inverter of the RC, all throttle valves, and the safety system communicate with the server via *Profibus DP*. The valves controlling the airflow of the air-film bearings (AFB) communicate via a serial interface. Temperature values are read by a temperature scanner, communicating with the server via *Modbus RTU*. The inlet throttle for sub-atmospheric operation is also controlled via a serial interface. Apart from these digital interfaces, several analog sensors are necessary to supervise the auxiliary systems. This data is directly read by an analog I/O card inserted into the control server.
For the auxiliary compressor, three remote I/O systems are distributed across the facility, controlling the motor controller of the AC, all sub-systems of the AC rig, and the two oil supply systems, one for the AC and one for the gearbox, respectively. The remote I/O systems are connected to the *Profibus DP* network. As for the RC, temperature values are read by a scanner and sent to the control server via *Modbus RTU*.
All realtime values are displayed to the rig operator on a graphical user interface (GUI) running on a separate PC in the control room. User inputs can be made on the same GUI, which are checked for feasibility and then forwarded to the actuators. PC and server communicate via the OPC UA protocol. This data interface is also used to feed operational data from the control system into the DAQ system.

Safety-related features run on a safety-certified PLC. The safety system includes monitoring all doors accessing the compressor rooms, the facility's power supply, the correct functionality of the control server, and the emergency-stop buttons. Data from the vibration monitoring system and stall detection is also forwarded to the safety system to control the emergency shutdown and opening of the anti-surge valve, respectively; see Section 6.3. A second safety-certified PLC is installed in the AC room. Both PLCs are interconnected via a dedicated serial communication line.

The control software is an in-house developed multi-threaded software programmed in C++. The main thread contains the initialization of all devices and the cyclic main program loop. This loop runs with a cycle time of 100 ms. Inside the loop, data from all sensors is read, processed, and checked for plausibility. Then, the operational limits of the test rig are checked. An emergency shutdown is triggered if limits are exceeded. All sensor values and the results of the checks are written to the OPC server. Then, control inputs from the user are forwarded to the actuators. Another thread runs the OPC server, which is responsible for data exchange with the control PC and the DAQ system.

6 INSTRUMENTATION AND MEASUREMENT SYSTEM

The research compressor is equipped with extensive instrumentation to investigate the overall performance and the flow field in detail. As temperature differences in a low-speed compressor are relatively small compared to the achievable measurement accuracy, measurements inside the *FRANCC* focus on pressure measurements.

6.1 Fixed Instrumentation

To investigate the operational behavior of the research compressor throughout the entire test, pressure and temperature instrumentation permanently integrated into the RC is used. Each measurement location carries a unique label, within which the axial position (measurement plane) is encoded as "Sxyz", where

- "x" is the index of the stage with 0 = inlet and IGV, 1-3 = compressor stages, 5 = outlet.
- "y" is the location inside the stage with 2 = upstream and 4 = downstream of a rotor blade, and 5 = upstream and 8 = downstream of a stator vane.
- "z" indicates if it is a fixed instrumentation (0) or a traversing location (5); see Section 6.2.

Figure 9 shows a meridional section of the gas path, including the fixed instrumentation. All measurement planes are labeled according to the abovementioned scheme.

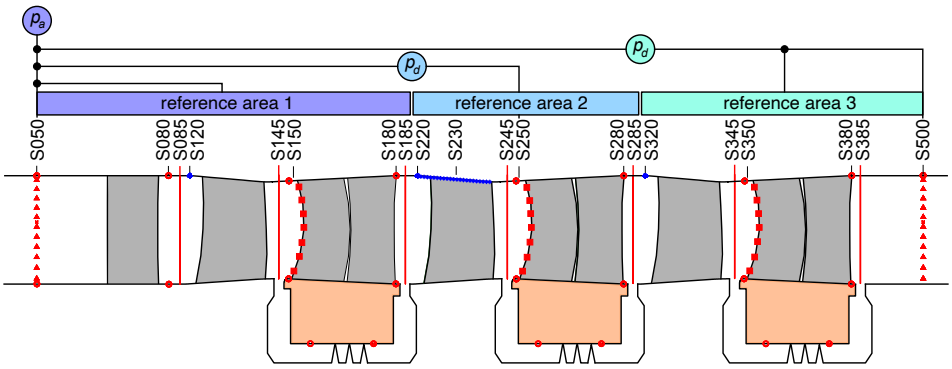

Figure 9 Instrumentation scheme of the research compressor, build 1.0

To investigate the overall compressor performance, three rakes with eleven radially distributed total pressure and one total temperature measurement at each rake are installed in both the inlet (S050) and outlet (S500). The static pressure is measured by six wall pressure taps at the hub and casing, respectively, at the same axial position as the rakes. A total of twelve static pressure taps are also installed at the exit of the IGV (S080). The front vane of one tandem stator of each stage is equipped with leading edge total pressure measurements (seven Kiel-heads per vane) and eight static pressure taps at the hub and casing platform (Sx50), respectively. Downstream of the stator, another set of twelve static pressure taps is installed (Sx80). With the static pressure measurements, the performance of the three compressor stages can be compared. Furthermore, the static pressure measured by aerodynamic probes can be validated.
Figure 10 shows stator vanes with fixed instrumentation. In Figure 10a, static pressure taps are located at the end walls. The picture shows all possible measurement positions, while in the real compressor, the different relative measurement locations are distributed over different vanes. One relative position with respect to the vane is identical on each instrumented vane to assess the circumferential uniformity of the flow. Figure 10b shows the Kiel-heads of the leading edge total pressure measurements. In the next build of the compressor (build 2.0), also blade surface pressure taps will be included, which are shown in Figure 10c. Build 2.0 will also include temperature sensors on the stator's leading edges to investigate the efficiencies of the three compressor stages.

Three static pressure measurement taps are located both upstream and downstream of the sealing fins of each stator cavity. Together with three temperature measurement locations inside the cavity, the leakage mass flow through the stator cavity can be computed. This information is of interest because the leakage flow has a significant effect on the performance and secondary flow phenomena of the tandem stator; see [7].
For unsteady measurements, nine fast-response pressure sensors are installed in the compressor. The current installation consists of three sensors in the casing upstream of the rotor tip of each compressor stage (Sx20). Being accessible from outside, the sensors can be re-positioned to 17 circumferential positions per stage

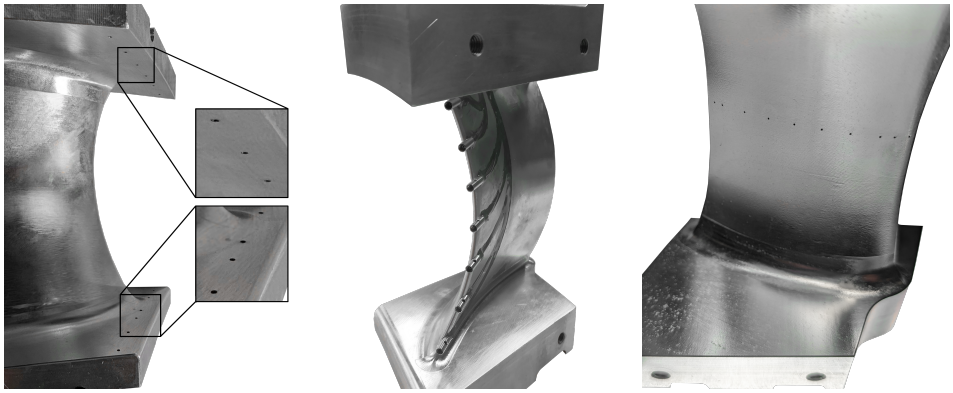

(a) Platform static pressure (b) Leading edge total pressure (c) Blade surface pressure

Figure 10 Instrumented stator vanes

in any combination without disassembling the compressor. The sensors can also be relocated into an array of 23 measurement locations in the casing over the entire length of rotor 2 (S230) to obtain the time-resolving pressure field of the rotor tip. Both the rotor and stator of stage 2 feature an optical access, which enables the use of optical measurement techniques such as Particle Image Velocimetry (PIV) or Laser Doppler Anemometry (LDA).

The steady-state pressure measurement system consists of 304 differential pressure channels distributed over two pressure ranges: 2.5 kPa (≈ 10 "WC) and 7.5 kPa (≈ 1 Psi). The used pressure sensors are the 9016 and 9116 series from *PSI/ Measurement Specialties, Inc.* as well as the *xPSC* from *SVMtec GmbH*. A specialty of this test rig is that an individual reference pressure sensor with high accuracy exists for each compressor stage, as depicted in Figure 9. This procedure allows using sensors of an identical small range everywhere inside the compressor. This improves the overall measurement accuracy significantly. The used sensors for the referencing system are *Mensor LP, CPT6020*, where an absolute pressure sensor (p_a in Figure 9) is used as the reference for stage 1 and differential pressure sensors (p_d) with a range of 150 mbar are used to reference stages 2 and 3 with respect to stage 1.
Temperatures are measured with two devices of the *Fluke Corporation, 2640A*. Each device allows connecting up to 20 thermocouples or 10 resistance thermometers in 4-wire configuration. The total temperature measurements at the inlet and outlet are performed with T-type thermocouples in the current setup. For the temperature measurement in the stator cavity, Pt100 sensors in 4-wire configuration are used.
The measurement setup is completed with the measurement of the rotational speed, torque, mass flow rate, and humidity. The rotational speed is taken from the inverter of the main drive, which measures the speed via an encoder with 2048 impulses per revolution. The torque is measured with the system *XtreMA* from *Manner Sensortelemetrie GmbH*. The torque measurement flange located between the main drive and the compressor consists of two measurement ranges, namely 2000 Nm and 400 Nm. The second measurement range is necessary to ensure the required measurement accuracy during sub-atmospheric operation. The mass flow is measured by a customized *Spindle Flowmeter* from *Vectoflow GmbH*, which is installed inside the exhaust duct between the volute and the throttling system. The flowmeter is calibrated in situ by flow measurements in the compressor's inlet duct. Lastly, the measurement of the humidity, performed with the sensor *BME280* from *Bosch Sensortec GmbH*, is used to account for changes in the gas properties of the working fluid, humid air; see Section 6.3.

No scientific investigations are planned at the auxiliary compressor itself. A basic set of instrumentation is still necessary to monitor the operating point and

prevent operation too close to any limit. At both the inlet and outlet ducts of the AC, static pressure taps are installed. Knowing the geometry and the mass flow, the total pressure ratio can be computed. Together with the mass flow, the current operating point can be drawn into the compressor map and monitored during operation. Additionally, the total temperatures at the inlet and outlet are measured so that the efficiency can be computed and the compressor operated at an optimal point. The rotational speed and torque of the AC are measured to prevent exceeding the limits of the drive train.

6.2 Traversing System and Aerodynamic Probes

Besides the fixed instrumentation, there are traversing planes downstream of each blade row, which allow traversing aerodynamic probes. The traversing locations are indicated in Figure 9 by red lines; the locations are named Sxy5. In each traversing plane, probes can be mounted on two sides of the compressor. Circumferential movement is possible in the $\pm 14°$ range on each side of the compressor, corresponding to a total of 6 flow passages for a blade count of 40. Due to the traversing slots located exactly above the stator cavity entrances/exits, it is possible to traverse the probe radially over the whole channel height behind all rotors and stators. Behind the IGV, no cavity exists (see Figure 9); following that, a margin has to be kept from the hub. No circumferential traversing is possible in the inlet section, but radial traverses can be installed at each of the six circumferential mounting positions for rakes. Also there, a safety margin from the hub must be held in. The aerodynamic probes are always prealigned to the estimated flow angle so that the measurement precision of the probes is used at their best.

The traversing system is controlled by an in-house software named *PythonDAQ-TraverseControl*. The software moves all axes simultaneously to the target positions specified in an input table. After a short waiting time (currently 6 s), which is necessary to settle the pressures in the measurement lines when using aerodynamic probes, the software triggers the DAQ system to record all measurement data for a specified duration (currently 5 s). Once the recording is completed, the software moves the axes to the next target position, and the recording pattern is repeated.

Currently, five-hole probes and a Kiel-type temperature probe for steady-state measurements, and hot-wire probes for time-resolved measurements are used. The different probe types are depicted in Figure 11. All probes are clamped in a probe holder and calibrated with this in the institute's calibration wind tunnel. The probe holder has a diameter of 13 mm to enable also large probes to be accommodated and has defined reference surfaces for aligning the probe in the compressor. To adjust the radial probe head position precisely to the probe used, the traverse's home position is set using a dummy probe.

The steady-state flow field measurements downstream of all blade rows are conducted using five-hole probes (5HP). Three of these probes can be used simultaneously (e.g., behind all rotors or all stators). The 5HPs have a pyramid head with a diameter of 1.7 mm (see Figure 11, bottom-left). They are calibrated in the range between $\pm 26°$ for the yaw angle and $\pm 20°$ for the pitch angle. Steps of $1°$ in general and steps of $0.5°$ in the $\pm 10°$ range are used. Eight Mach numbers between $Ma = 0.035$ and $Ma = 0.35$ are used for the calibration. A re-calibration in regular intervals provides a constant measurement accuracy even if the probe's aerodynamic performance degenerates with time.

For unsteady flow field measurements, hot-wire probes (HW) are used. A modified single-wire probe (based on the type 55P14 from *Dantec Dynamics A/S*) is used to determine the inlet conditions in terms of turbulent intensity and turbulent length scale. This HW probe uses a 1.25 mm long and 5-micrometer thin gold-plated

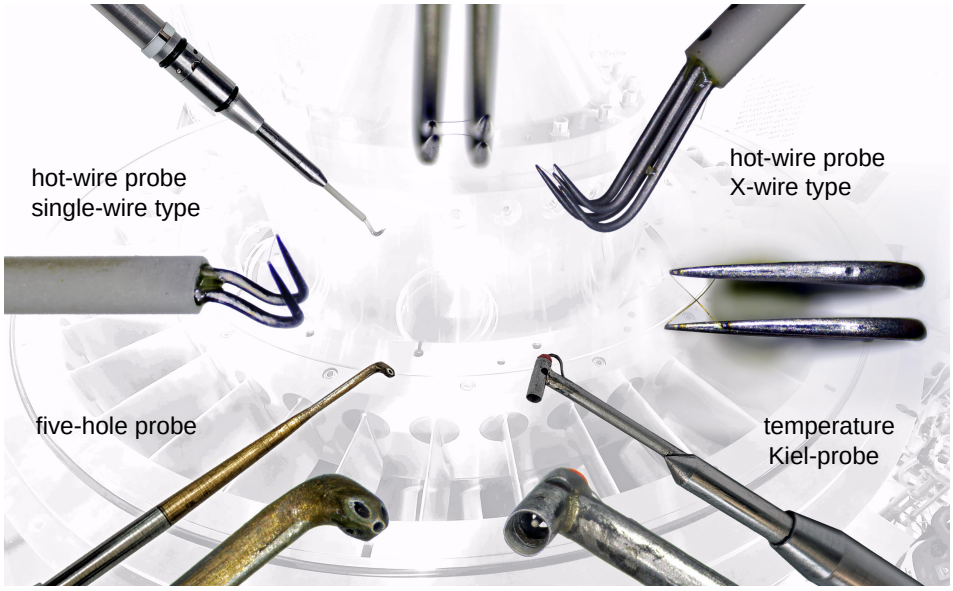

Figure 11 Aerodynamic probes

tungsten wire; see Figure 11, top-left.
X-wire probes (modified, based on the type 55P64 from *Dantec Dynamics A/S*; shown in Figure 11, top-right) are used for the measurements behind the blade rows. This allows both the mass flow density and the yaw angle to be determined unsteadyly. The wires of the probe are welded with less tension and a noticeable slack, as described in [16], to prevent disturbances on the measured signals due to prong vibrations causing strain gauging. X-wire measurements are used to resolve the time-dependent rotor and stator flow fields and, thus, enable the investigation of the rotor-stator and stator-rotor interactions of the new tandem vane configurations. They are calibrated in the range between $\pm 35°$ for the yaw angle. Steps of $1°$ in general and steps of $0.5°$ in the $\pm 10°$ range are used. Ten Mach numbers between $Ma \approx 0.00$ and $Ma = 0.35$ are used for the calibration.
A temperature Kiel-probe is simultaneously traversed in the same measurement plane at the same relative pitch with respect to the stator vanes when conducting measurements. This data is then used to correct errors due to changing temperatures during a test run (and also during calibration). This is necessary since *FRANCC* is an open-loop test rig, and weather and daytime conditions directly influence the incoming flow to the compressor.
The *StreamWare Pro* constant-temperature anemometry (CTA) system (also from *Dantec*) is used for all hot-wire measurements.

The temperature Kiel-probe (Figure 11, bottom-right) uses a mineral-insulated type T thermocouple (class 1) with 0.5 mm thickness. The Kiel-head has a diameter of 3 mm. Measurements at the calibration wind tunnel showed a recovery factor of 0.95 and fast responding behavior, even at low velocities.

6.3 Data Acquisition and Processing

The data acquisition system is a PC-based system with its core being the data server. All sensors are connected to the server via digital communication lines, mostly Ethernet, with different protocols. For the Ethernet, a backbone of 10G fiber optical lines is layed out throughout the facility. With fiber-optic to copper switches, which are located in the control and measurement cabinet, the AC room, and the control room, the sensors and PCs are then connected via gigabit copper Ethernet lines. Some sensors also use serial communication. Figure 12 shows the general layout of the DAQ system and serves as a visual reference for the following explanations.

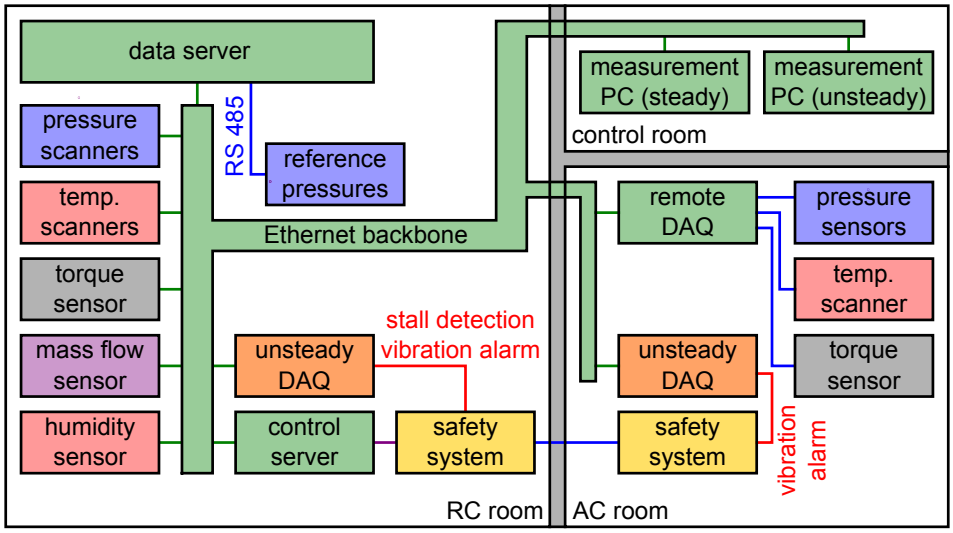

Figure 12 Structure of the measurement and DAQ system

All steady-state measurements are acquired via the in-house developed data acquisition software *PythonDAQ* [17]. The same software is also used for performing online computations, displaying data live, and the postprocessing of measured data.

The software consists of a data server application that connects to the sensors, as described above. In a cyclical task, the current measurement data is acquired from the sensors and used further to perform online computations. These computations are used in the *FRANCC* test rig extensively, as explained here:

First, the measured pressure values are combined with the referencing values according to the scheme explained in Section 6.1 and corrected for geodetic height differences. The correction is necessary because the geodetic height z of the measurement location "meas" and the sensor are unequal. The applied equation for the correction is based on the Bernoulli equation assuming a constant ambient temperature T_{amb} over the length of the pressure line:

$$p_{\mathrm{meas}} = p_{\mathrm{sensor}} \cdot \frac{g \cdot z_{\mathrm{sensor}} + R \cdot T_{\mathrm{amb}}}{g \cdot z_{\mathrm{meas}} + R \cdot T_{\mathrm{amb}}} \tag{1}$$

Temperature measurements are corrected by applying the recovery factor for each specific probe. After the corrections are applied, averaging techniques are used to compute scalar values from the individual measurement positions at each axial location of the compressor. This includes computing area-averaged values of the total pressure in the compressor's inlet and outlet, derived from the rake measurements.

As the last step, turbomachinery-specific parameters such as the total pressure ratio, corrected speed, corrected mass flow, efficiencies, the flow coefficient, and the work coefficient are computed. The total pressure ratio is calculated by directly comparing the area-averaged total pressure values from the inlet and outlet rakes, namely:

$$\Pi_t = \frac{\overline{p}_{t,\mathrm{S500}}}{\overline{p}_{t,\mathrm{S050}}} \tag{2}$$

The corrected rotational speed of the compressor is computed taking into account changes in the total inlet temperature and the gas properties due to the humidity of the intaken air, according to [18]:

$$n_{\mathrm{corr}} = n \cdot \sqrt{\frac{T_{\mathrm{ref}}}{\overline{T}_{t,\mathrm{S050}}}} \cdot \sqrt{\frac{\gamma_{\mathrm{ref}} \cdot R_{\mathrm{ref}}}{\gamma_{\mathrm{test}} \cdot R_{\mathrm{test}}}} \tag{3}$$

Analog, the corrected mass flow following the argumentation of [18] is defined as:

$$\dot{m}_{\mathrm{corr}} = \dot{m} \cdot \frac{\sqrt{\frac{\overline{T}_{t,\mathrm{S050}}}{T_{\mathrm{ref}}}}}{\frac{\overline{p}_{t,\mathrm{S050}}}{p_{\mathrm{ref}}}} \cdot \sqrt{\frac{\gamma_{\mathrm{ref}} \cdot R_{\mathrm{test}}}{\gamma_{\mathrm{test}} \cdot R_{\mathrm{ref}}}} \tag{4}$$

Equations 3 and 4 are simplifications assuming the influence of the inlet Mach number on the correction itself being neglectable, which is reasonable for the accounted inlet Mach numbers in the RC of smaller than 0.2. For a rigorous mathematical approach and a detailed discussion of the influences of certain assumptions, the reader is referred to [19]. The gas properties γ and R at test conditions are computed from a mixture of the properties of dry air and water vapor using the absolute humidity. Changes in the gas properties throughout the compressor are neglected as the temperature ratio in the low-speed machine is quite small. The compressor is operated in an open loop and, therefore, experiences changes in the ambient conditions (temperature, pressure, and humidity). To obtain an aerodynamically steady-state behavior, the mechanical speed is adjusted to keep the corrected speed constant throughout the test. The throttle setting is adjusted at the beginning of the test for the desired corrected mass flow and kept constant throughout the rest of the test.
For the efficiency of the compressor, several formulations can be considered. The general (temperature-based) formulation of the polytropic efficiency writes:

$$\eta_{\mathrm{pol,temp}} = \frac{\gamma - 1}{\gamma} \cdot \frac{\ln\left(\frac{\overline{p}_{t,\mathrm{S500}}}{\overline{p}_{t,\mathrm{S050}}}\right)}{\ln\left(\frac{\overline{T}_{t,\mathrm{S500}}}{\overline{T}_{t,\mathrm{S050}}}\right)} \tag{5}$$

Due to the measurement uncertainties of temperatures, this would lead to insufficiently accurate results; see Section 6.4. Therefore, the total temperature ratio is replaced with the specific mechanical work input, measured by speed (angular velocity ω), torque M, and mass flow $\dot{m}$:

$$\eta_{\mathrm{pol,torque}} = \frac{\gamma - 1}{\gamma} \cdot \frac{\ln\left(\frac{\overline{p}_{t,\mathrm{S500}}}{\overline{p}_{t,\mathrm{S050}}}\right)}{\ln\left(\frac{M \cdot \omega}{\dot{m} \cdot c_p \cdot \overline{T}_{t,\mathrm{S050}}} + 1\right)} \tag{6}$$

Equation 6 is the one which is used for all scientific evaluations on the *FRANCC* test rig. In other publications, the torque-based isentropic efficiency [4], [12], [5] or other unknown formulations [1] are used, so care has to be taken when comparing quantitative values from different test rigs. The fact that the torque and not the temperature ratio is taken for the evaluation of the efficiency is common to all the four mentioned publications.

All parameters are periodically written to a log file and made available on an OPC UA server run by *PythonDAQ*. Apart from the continuously written logfile, the measured values can also be written into a measurement file for a specified duration. This functionality is automatically used upon triggering by the traversing system or called manually when performing speedline measurements. [17]
For the online monitoring of the measured values, the GUI application *VisualizationClient* is part of the software package. This application runs on a PC in the test rig's control room and provides realtime display of numerical values and different kinds on live charts. [17]

Signals from fast-response pressure sensors are acquired by an unsteady measurement system from *Gantner Instruments GmbH* at a rate of 40 kSamples/s per channel. Given the blade-passing frequency of approx. 1 kHz, this rate provides a good resolution of the rotor's pressure field. The same system also acquires data from the vibration and shaft position sensors installed inside the RC. Furthermore, two trigger signals with one and 120 impulses per revolution, respectively, are recorded. The impulse signals are used for data matching in the postprocessing

phase of experiments.
The raw data is further processed on the system's signal processor: RMS values of all channels are computed at regular intervals. These values are monitored for exceeding specified limits: Stall of the compressor is detected if the RMS limit of any of the fast-response pressure sensors is exceeded. This automatically triggers the opening of the anti-surge valve and the fast-opening mechanism of the main throttle valve. Because of this measure, the compressor recovers from stall within less than five seconds. If RMS limits of the vibration or shaft position sensors are exceeded, a mechanical issue is likely. Therefore, a shutdown of the facility is triggered automatically.
All measured data is sent from the signal processor to a PC in the control room via Ethernet. There, the values are displayed to the operators of the test rig. On the same PC, all raw data values are continuously recorded. Computed values, such as the RMS values, are not recorded to save disk space. These values can be re-calculated at any time in the postprocessing phase from the raw data.

Sensors installed in the auxiliary compressor facility are integrated into the same DAQ system. In this case, the three installed sensor types, pressure, temperature, and torque sensors, all account for a serial communication interface. These interfaces are read by a remote DAQ device and transferred into Ethernet signals. The data server connects to the remote DAQ and reads the measurement values.
In the AC room, a vibration monitoring system from *IfTA Systems GmbH* is installed, which monitors both linear and torsional vibrations of the drive train and the compressor. Analog to the RC, vibration metrics are computed and compared against limit values. An alarm is forwarded to the AC's safety system if a limit is exceeded. The safety systems of RC and AC are interconnected (see Figure 12) so that a controlled shutdown of the whole facility is possible.

In the postprocessing phase of experiments, mainly the triggered measurements (see description above) of a steady state operating point are used. The postprocessing normally contains the following steps:

1. Read the measurement files.
2. Reduce and combine data, e.g., time averaging of steady-state measurements or combining individual traverse points to a matrix.
3. Compute further flow quantities from the measurements or compute flow quantities from aerodynamic probe measurements.
4. Plot the data into human-interpretable graphical representations.

For each of the mentioned evaluation steps, predefined classes and functions are included in the *PythonDAQ* package. These are combined individually for a specific experiment in a postprocessing *Python* script. [17]

Five-hole probes are used in the non-nulling mode. Therefore, a calibration, as explained in Section 6.2, is necessary. Calibration is performed at several Mach numbers to compensate for Reynolds number effects. For each Mach number, the four calibration coefficients C_α, C_β, C_t, and C_s according to [20] are computed from the measured pressure values. The coefficients are stored together with the known flow conditions in calibration tables.
To postprocess data from the compressor experiments, an algorithm similar to the one presented in [20] is used. The coefficients C_α and C_β are directly derived from the five pressure readings. To compute the flow angles, total and static pressures, the calibration tables are interpolated with splines assuming a certain Mach number. The equation system can be closed by computing the Mach number via the derived total and static pressure. As described in [20], the procedure requires iteration until the computed Mach number converges. The calibration tables are interpolated to the current Mach number at each iteration, which has an affordable

computational cost on a modern PC. The algorithm to postprocess measurement data from five-hole probes, together with routines for the data handling and plotting of the results, are implemented as classes in the *PythonDAQ* package.
The evaluation algorithm tends to produce large, unphysical "spikes" in the flow angles when large gradients of the flow velocity throughout the extension of the probe head are present as described in [21]. The reason is that by comparing the pressure on two opposite holes of the probe, the standard evaluation algorithm cannot distinguish between a flow angle and a velocity gradient. These artifacts usually occur when the probe enters or exits the wake of a stator vane or when any of the sidewalls is approached. The extension of the "spikes" can be reduced to an acceptable level with the shear flow correction proposed in [21]. Based on the geometry of the probe head and the present velocity gradient, the "angle", which is erroneously determined by the probe evaluation, is computed. This angle error is then subtracted from the computed flow angle to obtain a realistic measurement value. The correction algorithm is integrated into the probe evaluation program and can be turned on or off by the user.

For the hot-wire measurements, the anemometer voltages of the CTA are measured by a stand-alone data acquisition device *NI USB-6218* from the *National Instruments Corporation*. For the subsequent matching process, a trigger signal is also recorded, which is triggered once per rotor revolution. Two seconds are recorded per measurement point at a rate of 70 kHz. A low-pass filter of 30 kHz is used for the hot-wire anemometer to avoid aliasing effects. The values are chosen based on the blade-passing frequency of the compressor, considering the available options of the CTA system. The measured anemometer voltages are then subjected to a correction to minimize the influence of temperature fluctuations during calibration and the test run. For the single-wire measurements in the compressor inlet, the average temperature from the inlet rakes is used for this purpose. For the X-wire measurements between the blade rows, the temperature from the Kiel-probe measurements (see Section 6.2) is used.
The corrected voltages are then fed to the calibration functions to calculate the mass flow density and, for X-wire measurements, also the yaw angle. For HW measurements, polynomials are used as calibration functions. Sixth-order polynomials have proven suitable for single-wire measurements. Fifth-order polynomials proved to be optimal for X-wire measurements. Several calibration functions were investigated at the institute, with polynomial functions proving to be superior. This is also in line with a previous study on parallel hot-wire probes [16]. For the temperature correction, the method of [22] is implemented:

$$E_{\text{corrected}} = \left(\frac{T_{\text{wire,hot}} - T_{\text{reference}}}{T_{\text{wire,hot}} - T_{\text{ambient}}} \right)^{n} \cdot E_{\text{acquired}} \tag{7}$$

The correction is valid for a temperature change of up to 10°C. This can be extended by modifying the exponent n (suggested in [23]), which is normally set to 0.5. This factor is determined by conducting additional test runs at the calibration wind tunnel with different flow temperatures using a heater.

6.4 Measurement Uncertainties

Measurement uncertainties of both directly measured and computed quantities are determined by applying the method by JCGM GUM [24] and [25]. The uncertainties are derived theoretically, starting from the information given in the datasheets of all measurement devices and using the formulae for uncertainty propagation. This approach follows the concept of method B by GUM [24]. The procedure for determining the uncertainty of turbomachinery-specific quantities consists of the following steps; cf., [25]:

1. Take uncertainty values from the datasheets of the sensors and measurement devices.
2. Compute the standard uncertainties from the given values, taking into account the individual probability distributions.
3. Combine the contributions to the uncertainties (e.g., sensor, cable, and measurement device) of the individual measurement readings by a sum of squares.
4. Combine the uncertainties of the individual readings to the uncertainties of the turbomachinery-specific values, which are described in Section 6.3. The combination process is described in ([25], Clause 5.1). The underlying assumptions are that all uncertainty contributions are uncorrelated and a linearization for the problem is justified. The linearization point is the aerodynamic design point of the 3.5-stage compressor; see Table 1.
5. Compute the expanded uncertainty with a coverage factor of $k = 2$, which corresponds to a level of confidence of approx. 95 %.

Table 2 shows the expanded uncertainties for a selection of the most important measurement values from the fixed instrumentation. Values are rounded to two digits. It can be clearly seen that the temperature-based efficiency value is far off a reasonable uncertainty while the torque-based is within. Furthermore, it has to be noted that these values are theoretically derived and, therefore, conservative. The experience from the measurements shows that the temperature-based and torque-based efficiency values usually lay within 2 % to each other. Comprehensive uncertainty estimations for test rigs are rarely found in the open literature. Values are given, e.g., for the test rig in Dresden. The uncertainty values of the *FRANCC* are higher than the ones listed in [4]. The main contributor to a higher uncertainty of the efficiency is the mass flow, which itself is dependent on the accuracy of the in-house calibration. For the same test rig in Dresden, [12] shows values more comparable to those in Table 2. This suggests that the theoretical derivation, although conservative, is a good indicator of the long-term achievable accuracy.

Table 2
Expanded measurement uncertainties (k = 2) for the fixed instrumentation at atmospheric operation

Quantity	Symbol	Absolute Uncertainty	Relative Uncertainty
Differential pressure reading	$\Delta p_{\text{sens-ref}}$	± 12 Pa	± 0.17 %
Abs. pressure after referencing	p_{meas}	± 25 Pa	± 0.026 %
Temperature	T	± 1.0 K	± 0.35 %
Total pressure ratio	Π_t	± 0.00036	± 0.032 %
Corrected speed	n_{corr}	$\pm 2.6 \frac{1}{\text{min}}$	± 0.17 %
Corrected mass flow	$\dot{m}_{\text{corr}}$	$\pm 0.16 \frac{\text{kg}}{\text{s}}$	± 0.89 %
Temp.-based polytropic efficiency	$\eta_{\text{pol,temp}}$	± 12 %	
Torque-based polytropic efficiency	$\eta_{\text{pol,torque}}$	± 0.96 %	

At sub-atmospheric operation, the measurement uncertainties are slightly higher because not all measurement ranges are used to their full extent. Countermeasures, such as the two ranges for the torque sensor, lead to reasonable uncertainties even for the sub-atmospheric operating points.

The measurement accuracy of the five-hole probe cannot be derived analytically because of the iterative algorithm explained in Section 6.3 and the involved interpolation schemes. Therefore, a numerical propagation of the uncertainty distribution applying the Monte-Carlo method [24], [26] is used. Uncertainties of the calibration facility have to be taken into account as well. For the hot-wire probes,

the uncertainty is subject to various influences. The investigations for both probe types are ongoing and will be presented in a future publication. The uncertainty of the temperature Kiel-probe is the same as for fixed temperature measurements; see Table 2.

7 MEASUREMENT RESULTS

The research compressor had its first run in December 2021, followed by a commissioning phase, which included the necessary in-situ calibration of the mass flow sensor. Scientific investigations on build 1.0, introduced in Section 3, consisting of conventional (single-blade) rotors and tandem stator vanes, have been ongoing since January 2023. In this section, the overall performance of the 3.5-stage compressor at design speed and flow field measurements at design operating conditions are presented. All measurement data is compared with CFD simulations, which are obtained with a 3.5-stage model including the stator cavity, all gaps, and fillets. The simulations are carried out as steady-state RANS simulations with the solver *Numeca FineOpen 11.1*. Turbulence is modeled with the Spalart-Allmaras model because this single-equation model covers the flow phenomena well while being less computationally intensive than models with two equations. The flow field is evaluated at the same locations where the measurements are taken. A detailed discussion of the measurement and simulation results can be found in the project report [27].

Figure 13 shows the overall compressor performance at 100 % corrected design speed compared to the CFD results. The upper part of the figure shows the total pressure ratio over the corrected mass flow, and the lower part shows the polytropic efficiency. At first glance, it can be observed that the trend of the total pressure ratio is covered well by the simulation but with a small offset to the experimental data. The reason for this is still under evaluation. A measurement error can be excluded as the outflow angles of the rotors also have the same systematic difference. The operating range of the compressor, i.e., the stall limit, is predicted very well by the numerical simulation.
The efficiency plots of the experiment and CFD also show an offset. The offset in efficiency is a direct consequence of the lower pressure ratio predicted by the CFD while the work input is comparable. It has to be noted at this point that the computation of the efficiency for the low-speed machine is very sensitive to changes in raw data values. The maximum efficiency observed in the experiment lies approximately at the same total pressure ratio of the machine as for the CFD, but because of the higher pressure ratio of the experiment, this point lies at approx. 108 % corrected design mass flow.
The single-stage test of a similar configuration at TU Dresden [12] shows comparable trends. Also there, the measured total pressure ratio has a certain offset to the CFD. The measured efficiency curve in [12] shows an asymmetrical behavior with a flat slope towards higher throttling and a steeper slope towards de-throttling. This behavior is also found in the present 3.5-stage setup. The reason is that tandem stators show a particular sensitivity towards negative incidence angles. [27]

Figure 14 shows radial plots of the circumferentially averaged axial Mach number and the absolute flow angle α at the exits of all tandem stators, where $\alpha = 90°$ represents axial flow. The data is obtained from steady-state 5HP measurements at the operating point where the design pressure ratio is reached. For comparison, simulation data at the same corrected mass flow for tandem stator 1 is included in the plot. Generally, a very good agreement between the experiment and simulation can be seen. This proves that the CFD setup is capable of predicting the flow structures accurately despite the differences of performance parameters observed in Figure 13. The axial Mach number plot in Figure 14a shows quite a "round" profile, i.e., thick end wall boundary layers. This is caused by the inten-

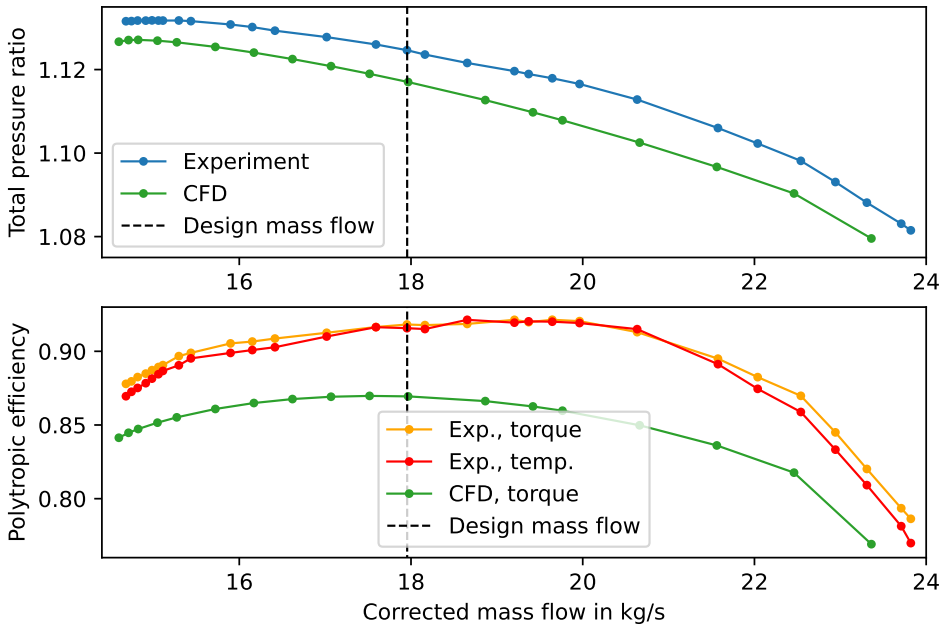

Figure 13 Compressor performance at corrected design speed

sive secondary flow structures of the tandem stator. The wider extension of the secondary flow structures seen in the experiment at the hub and the casing lead to an even more "round" profile compared to the CFD. The CFD underestimates the extension of the secondary flow structures for this operating point. It can be seen that the axial Mach number is gradually decreasing throughout the multistage machine. This is caused by the compressibility of the flow while the channel and blade geometry remain identical for all stages.

The plot of the absolute flow angle shows an almost identical shape between the experiment and CFD. Over a wide region of the span, the outflow angle is almost constant, indicating the proper design of the tandem stator for this operating point. At a radius of approx. 530 mm local differences between the experiment and CFD are visible. These are a direct consequence of the different extensions of the secondary flows. The shape of the flow angle profile is fairly identical for all stages. Differences can be observed in the hub region. Furthermore, a slightly higher deviation is observed for tandem stator 3. [27]

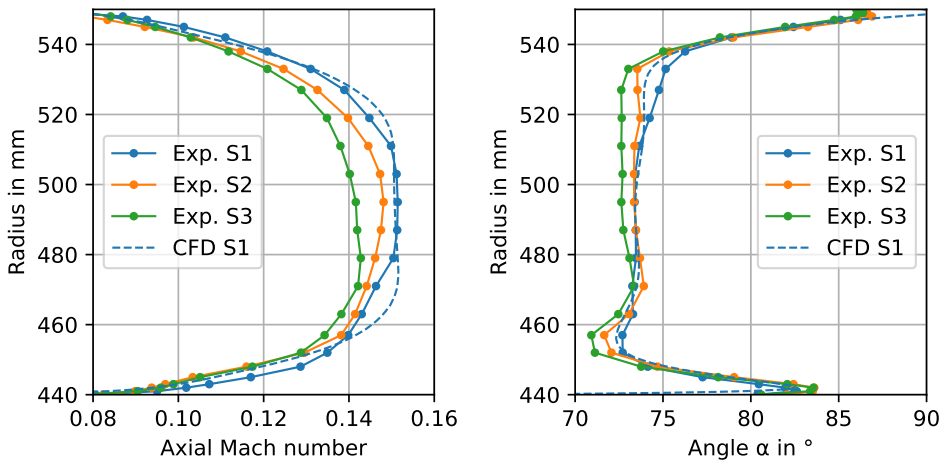

(a) Axial Mach number

(b) Absolute flow angle

Figure 14 Radial flow profile of the tandem stator outflow

8 CONCLUSION AND OUTLOOK

This paper presents the newly built low-speed axial compressor test rig *FRANCC*. The aim of the test rig is to investigate highly loaded compressor designs with new blading concepts, such as tandem and hybrid blades, in a representative environment. As the compressor counts 3.5 stages, the multistage behavior of these new concepts can be studied. A specialty is the possibility of lowering the inlet pressure via a throttle to 250 mbar to investigate the influence of the Reynolds number.
Extensive fixed instrumentation enables the assessment of the performance. With traversing planes downstream of each blade row, the flow fields can be investigated in detail with different kinds of aerodynamic probes. Steady-state measurements are performed with five-hole probes; unsteady measurements are taken with hot-wire probes. An optical access to the second compressor stage allows the application of optical measurement techniques.

The research compressor has been in operation since the end of 2021. The first measurement campaign (build 1.0) is finished by the time of the publication of this paper. First measurement results are discussed and show a very good agreement of the operational behavior and flow structures between the measurement results and numerical post-test CFD simulations.

In the course of the year 2024, the blading will be changed to the second build consisting of hybrid rotors, similar to the one shown in [28], and tandem stators. The auxiliary compressor and the inlet throttling system will be tested for the first time in the near future.

ACKNOWLEDGMENTS

The installation of the compressor test rig is funded by the Deutsche Forschungsgemeinschaft (DFG, German Research Foundation) – INST95/1446-1 FUGG.
The aerodynamic design of the research compressor, as well as the dedicated numerical and experimental investigations, are performed in the context of the research project "Unsteady Tandem Flow", funded by the Deutsche Forschungsgemeinschaft (DFG, German Research Foundation) – 420268957 and the FVV eV – 601360. The project working group is acknowledged for their continuous advice and support throughout the project.
The authors would like to express their special thanks to Marcel Schmieder for his immense effort in the design, buildup, and commissioning of the *FRANCC* test rig, Katharina Bär for the design and buildup of the auxiliary compressor system, Ralf Priller for making the in-house manufacturing of the compressor blades possible and Jannik Eckel for supporting the project with various CFD simulations, especially the post-test simulations enabling the scientific validation of the research compressor. Furthermore, the authors thank the whole team of the LTF and external people supporting the project with their expertise, great discussions, and ideas.

REFERENCES

[1] D. C. Wisler, "Loss reduction in axial-flow compressors through low-speed model testing," in *ASME 29th International Gas Turbine Conference and Exhibit*, no. 84-GT-184, (Amsterdam, The Netherlands), 1984.

[2] C. A. Wasserbauer, H. F. Weaver, and R. G. Senyitko, "NASA low-speed axial compressor for fundamental research," Tech. Rep. NASA Technical Memorandum 4635, National Aeronautics and Space Administration, Brookpark, Ohio, USA, 1995.

[3] Y. S. Li and N. A. Cumpsty, "Mixing in axial flow compressors: Part I — Test facilities and measurements in a four-stage compressor," in *ASME Gas Turbine and Aeroengine Congress and Exposition*, no. 90-GT-38, (Brussels, Belgium), 1990.

[4] P. Boos, H. Möckel, J. M. Henne, and R. Selmeier, "Flow measurement in a multistage large scale low speed axial flow research compressor," in *ASME International Gas Turbine & Aeroengine Congress & Exhibition*, no. 98-GT-432, (Stockholm, Sweden), 1998.

[5] B. Liu, C. Zhang, G. An, D. Fu, and X. Yu, "Using tandem blades to break loading limit of highly loaded axial compressors," *Chinese Journal of Aeronautics*, no. 35(4), 2022.

[6] M. Hopfinger and V. Gümmer, "Preliminary design of a three-stage low-speed research compressor using tandem vanes," in *AIAA Propulsion and Energy 2019 Forum*, (Indianapolis, Indiana, USA), 2019.

[7] M. Hopfinger and V. Gümmer, "Numerical investigations of stator shroud leakage effects in a 1.5-stage low-speed axial compressor," in *Proceedings of 14th European Conference on Turbomachinery Fluid Dynamics & Thermodynamics*, no. ETC2021-576, (Gdansk, Poland), 2021.

[8] M. Hopfinger and V. Gümmer, "Endwall boundary layer development in a multistage low-speed compressor with tandem stator vanes," in *Proceedings of the ASME Turbo Expo 2021: Turbomachinery Technical Conference and Exposition*, no. GT2021-58742, (Virtual, Online), 2021.

[9] P. von Jeinsen, J. Eckel, S. Giannini, and V. Gümmer, "A numerical design space investigation of low-speed axial compressor stages using single-row and tandem bladings," in *Proceedings of the ASME Turbo Expo 2023: Turbomachinery Technical Conference and Exposition*, no. GT2023-101948, (Boston, Massachusetts, USA), 2023.

[10] H.-A. Schreiber, W. Steinert, and B. Küsters, "Effects of reynolds number and free-stream turbulence on boundary layer transition in a compressor cascade," *Journal of Turbomachinery*, vol. 124, 2002.

[11] L. Reisinger, P. Bieli, and V. Gümmer, "Numerical analysis of the boundary layer behavior of low-speed linear cascade compressor airfoils with single and tandem configurations," in *Proceedings of ASME Turbo Expo 2024: Turbomachinery Technical Conference and Exposition*, no. GT2024-128813, (London, United Kingdom), 2024.

[12] A. Tesch, M. Lange, K. Vogeler, J. Ortmanns, E. Johann, and V. Gümmer, "An experimental investigation of a tandem stator flow characteristic in a low speed axial research compressor," in *Proceedings of ASME Turbo Expo 2014: Turbine Technical Conference and Exposition*, no. GT2014-26104, (Düsseldorf, Germany), 2014.

[13] "Measurement of fluid flow by means of pressure differential devices inserted in circular cross-section conduits running full - Part 1: General principles and requirements." ISO 5167-1:2022, 2022.

[14] "Measurement of fluid flow by means of pressure differential devices inserted in circular cross-section conduits running full - Part 2: Orifice plates." ISO 5167-2:2022, 2022.

[15] J. Kurzke *et al.*, "Gasturb 14." `www.gasturb.com`, 2022.

[16] C. Schäffer, A. Rabl, K. Speck, K. Boetzel, C. Helcig, and V. Gümmer, "Challenges in the application of hot-wire anemometry for the investigation of transient temperature fluctuations in a high-speed research compressor," in *Proceedings of the ASME Turbo Expo 2023: Turbomachinery Technical Conference and Exposition*, no. GT2023-100970, (Boston, Massachusetts, USA), 2023.

[17] D. Jäger and V. Gümmer, "PythonDAQ — A Python based measurement data acquisition and processing software," in *XXVI Biennial Symposium on Measuring Techniques in Turbomachinery, Transonic and Supersonic Flow in Cascades and Turbomachines*, (Pisa, Italy), 2022.

[18] J. C. Samuels and B. M. Gale, "Effects of humidity on performance of turbojet engines," Tech. Rep. Technical Note 2119, National Advisory Committee for Aeronautics, Cleveland, Ohio, USA, 1950.

[19] AGARD, "Recommended practices for the assessment of the effects of atmospheric water ingestion on the performance and operability of gas turbine engines," Tech. Rep. AGARD Advisory Report No. 332, Advisory Group for Aerospace Research & Development, 1995.

[20] A. L. Treaster and A. M. Yocum, "The calibration and application of five-hole probes," in *24th International Instrumentation Symposium: Instrumentation in the Aerospace Industry*, (Albuquerque, New Mexico, USA), Instrument Society of America, 1978.

[21] R. Willinger and H. Haselbacher, "A three-hole pressure probe exposed to velocity gradient effects – Experimental calibration and numerical investigaton," in *Conference on Modelling Fluid Flow (CMFF'03): The 12th International Conference on Fluid Flow Technologies*, (Budapest, Hungary), 2003.

[22] P. W. Bearman, "Corrections for the effect of ambient temperature drift on hot-wire measurements in incompressible flow," *DISA Inf.*, no. 11, 1971.

[23] F. E. Jorgensen, *How to measure turbulence with hot-wire anemometers – A basic guide*. Dantec Dynamics A/S, 2004.

[24] BIPM, IEC, IFCC, ILAC, ISO, IUPAC, IUPAP, and OIML, "Guide to the expression of uncertainty in measurement — Part 1: Introduction." Joint Committee for Guides in Metrology, JCGM GUM-1:2023, 2023.

[25] BIPM, IEC, IFCC, ILAC, ISO, IUPAC, IUPAP, and OIML, "Evaluation of measurement data — Guide to the expression of uncertainty in measurement." Joint Committee for Guides in Metrology, JCGM 100:2008, 2008.

[26] BIPM, IEC, IFCC, ILAC, ISO, IUPAC, IUPAP, and OIML, "Evaluation of measurement data — Supplement 1 to the "Guide to the expression of uncertainty in measurement" — Propagation of distributions using a Monte Carlo method." Joint Committee for Guides in Metrology, JCGM 101:2008, 2008.

[27] D. Jäger, M. Hopfinger, and V. Gümmer, "Unsteady tandem flow – Final report," in *The FVV Transfer + Networking Event — Information Sessions – Spring 2024*, vol. R608, 2024.

[28] J. Eckel, P. von Jeinsen, and V. Gümmer, "Numerical investigation of near-tip modifications for a highly loaded low-speed rotor under the influence of double leakage," in *Proceedings of the ASME Turbo Expo 2022: Turbomachinery Technical Conference and Exposition*, no. GT2022-82143, (Rotterdam, Netherlands), 2022.